POLITECNICO
MILANO 1863

SCUOLA DI INGEGNERIA INDUSTRIALE
E DELL'INFORMAZIONE

Executive Summary of the Thesis

Characterization of thermal behavior and surface properties of C_8-BTBT-C_8 by means of molecular dynamics simulations.

Laurea Magistrale in Materials Engineering and Nanotechnology

Author: Simone Provenzano

Advisor: Prof. Mosè Casalegno

Academic year: 2020-2021

1. Introduction

Organic materials for electronics and energy, considered a novelty just some decades ago, are now routinely employed in organic solar cells (OSCs), organic light-emitting diodes (OLED) displays and organic thin film transistors (OTFTs) development. The research on these materials, now well established, aims at improving device performance while scaling up the manufacturing process. In thin films applications, organic materials are deposited onto inert substrates, which may subsequently be engineered during device manufacture. Common techniques include spin-coating, ink-jet printing and vapour deposition techniques. The organization of the structures resulting from the deposition process, at the molecular level, has a major influence on the electron transport properties, and, in turn, on device performance.
Organic semiconductors can be broadly categorized into semiconducting polymers and small semiconducting molecules. Semiconducting polymers are the most widely studied and already applied in many commercialized solutions. They include Poly(acetylenes, Poly(p-phenylene vinylene)s, Poly(pyrrole)s, Polyanilines, Poly(thiophene)s and others.

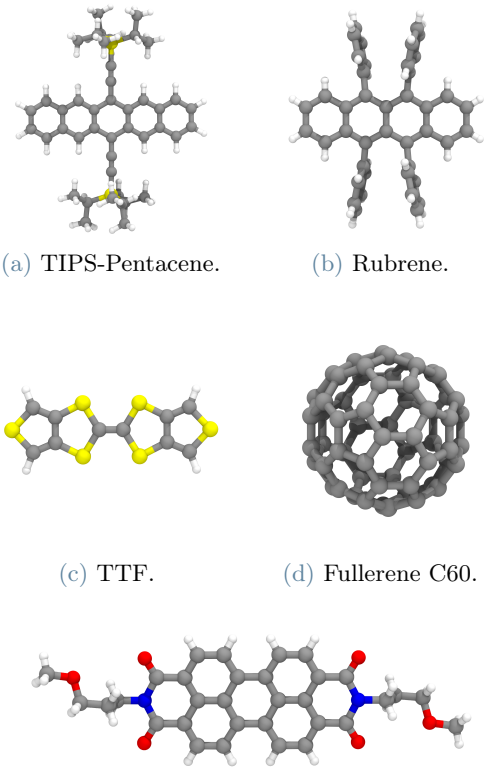

(a) TIPS-Pentacene. (b) Rubrene. (c) TTF. (d) Fullerene C60. (e) A PDCI derivative.

Figure 1: The "ball and stick" structure of some common small molecule semiconductors [1–5]. C is gray, H is white, S is yellow, O is red, N is blue, Br is pink and F is green.

Small molecules, conversely, are non-polymeric compounds, such as acenes, oligothiophenes, perylenes, diketopyrrolopyrroles, fullerenes and others (Fig. 1). Some small semiconducting molecules are liquid crystals (LC), thus characterized by phases between the liquid and the solid states. This property can be exploited with the aim of controlling the molecular structure, towards the development of the best conducting polymorphs. This class of materials includes the Benzothieno[3,2-*b*][1]benzothiophene (BTBT) family of moieties. These compounds share a conjugated core consisting of two thiophene rings and two terminal benzene rings. The various different species are characterized by their terminal group, which imparts different additional properties, like solubility. Among the best candidates for electronic applications from this family, 2,7-Dioctyl[1]benzothieno[3,2-*b*][1]benzothiophene (C_8-BTBT-C_8), has attracted a considerable deal of interest, due to its good electron transport properties (peak electron mobility exceeding 1 $cm^2(Vs)^{-1}$). The molecule features two terminal alkyl chains, to increase its solubility in common organic solvents. The crystalline cell and a detail on the molecular herringbone packing of the crystal are reported in Fig. 2 [6]. This material self organizes into crystalline layers, transitions to a smectic A phase at 380 K and to liquid at 396 K [7]. The aim of this work is obtaining a deeper understanding of this molecule's thermal behaviour and the effects of the presence of an amorphous silica surface on its layered structure. This is achieved through molecular dynamics (MD) simulations.

2. Molecular dynamics

Molecular dynamics (MD) is a powerful computational method to simulate the dynamic trajectory of a system of atoms, treated classically. This is achieved thanks to the Born-Oppenheimer approximation, which allows the separation of the solution of the electron dynamics, which is treated in terms of a mean field, from the dynamics of the atomic nuclei. If the simulation is long enough, it is possible to assume that the simulated system will visit all accessible configurations. Then, a variety of properties of the system can be obtained statistically from molecular trajectories.

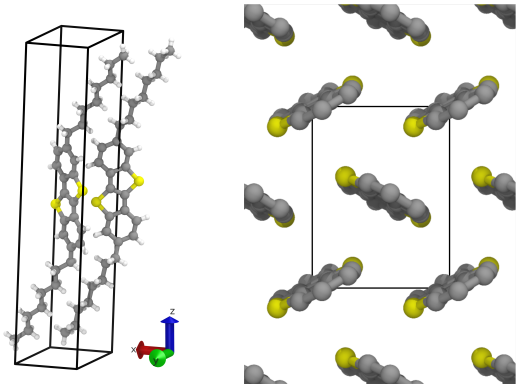

(a) Crystalline cell of C_8-BTBT-C_8.

(b) Herringbone packing motif.

Figure 2: Crystalline cell (a) and herringbone packing (b) of the C_8-BTBT-C_8 molecular crystal. The hydrogen atoms and the alkyl chains in (b) have been removed for clarity.

The interactions between the atoms are modelled through a potential, referred to as Force Field (FF), which consists in a sum of different terms for each type of interaction. These are used to determine the acceleration on each atom, thus velocity and positions.

3. Results and discussion

The MD simulations were performed with the GROMACS 2021.2 package [8]. Several steps are needed before proceeding with the simulations of the C_8-BTBT-C_8 crystals. The first one is the development of the FF, which was derived starting from the CHARMM 2021 FF. The CHARMM parametrization scheme was used for C_8-BTBT-C_8, CHARMM parameters for amorphous silica surfaces are available in the literature [9]. After some processing steps the FF was ready to be used.

3.1. System assembly and Numerical methods

The following step is the preparation of the inputs. The C_8-BTBT-C_8 systems simulated in this work stem from four input structures: a bulk periodic crystal, consisting in a supercell obtained replicating the crystalline cell 25 times, (BTBT_50) and three different C_8-BTBT-C_8 layers (derived from BTBT_50) positioned on an amorphous silica surface with 4.7 silanol groups per nm^2 (Q47_200, Q47_450, Q47_900) (Fig. 3, 4, 5, 6).

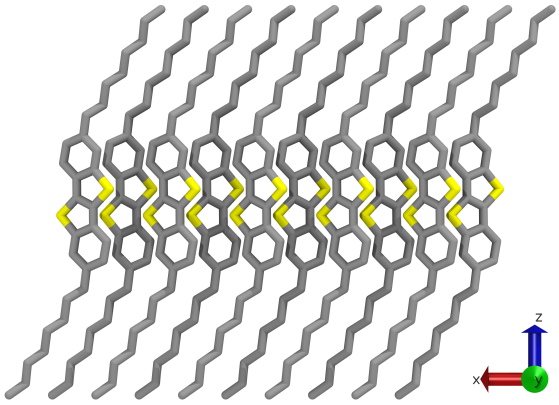

(a) Side view of the BTBT supercell.

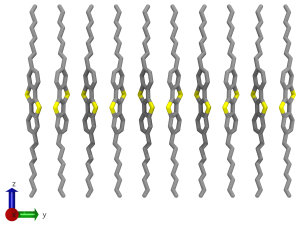

(b) Front view of the BTBT supercell.

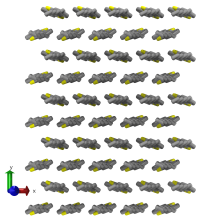

(c) Top view of the BTBT supercell.

Figure 3: Three different projections of the C_8-BTBT-C_8 supercell, consisting in 50 molecules. In (c) the point of view angle is tilted by 15° to highlight the herringbone motif.

All simulations have been performed with a time step of 1 fs. The simulations on the Q47 systems were performed with an orthorhombic box of height 25 nm, while the simulations on the bulk were performed under a NPT ensemble, so a thermostat and a barostat need to be used. The velocity rescaling thermostat has been used for the control of temperature (coupling constant of 1 ps). For the control of pressure (constant at 1 atm), the Parrinello-Rahman and Berendsen barostats have been used. The first one, with a coupling constant of 10 ps, was used in the BTBT_50 simulation at room temperature and on all the Q47 simulations, the second one, with a constant of 5 ps on the remaining BTBT_50 simulations. PBC were applied in all directions and the PME method was used to treat electrostatic interactions, with a grid spacing of 0.12 nm. A cutoff of 1.2 nm was applied to non-bonded interactions.

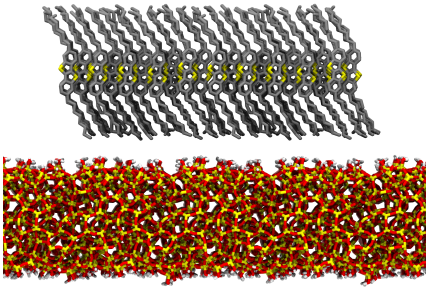

Figure 4: Front view of the Q47_200 system, assembled from 4 replicas of the supercell and the silica surface. Hydrogens were removed for representation.

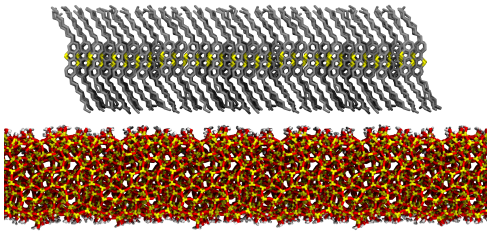

Figure 5: Front view of the Q47_450 system, assembled from 9 replicas of the supercell and the silica surface.

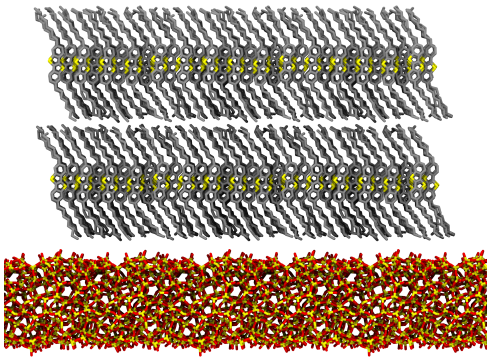

Figure 6: Front view of the Q47_900 system, assembled from 2 replicas of the Q47_450 BTBT layer and the silica surface.

The computational resources needed for the simulations were provided by the CINECA HPC consortium, after the submission of a ISCRA-C project. The resources included 108000 core hours on the GALILEO100 cluster [10]. The NumPy, Pandas and Matplotlib libraries for data analysis with Python [11–14] and the Vi-

sual Molecular Dynamics program for visualization were also used [15]. Densities and box dimensions were read form the trajectory data. The order parameter (S) was calculated to characterize the reciprocal molecular orientation in ordered and partially ordered phases. The following equation was used:

$$S = \frac{1}{2}\langle 3\cos^2\theta - 1\rangle \quad (1)$$

where θ is the angle between the molecular axis and the z axis. The angle is calculated from the coordinates of each molecule and the average is taken for each frame in a 30 Å by 30 Å area. The values of S range from -1.5 for completely deflected molecules, to 1 for aligned molecules. If S averages at 0, the molecules are randomly oriented and the system is isotropic. The height was calculated as the average of the maximum z coordinate of each molecule, subtracted of the average z coordinate of the surface (silanol groups taken as reference), again in a 30 Å x 30 Å area. Of these observables, all the time series are recorded in a CSV file.

3.2. BTBT_50: room temperature and force field validation

The first simulation has been performed on the BTBT_50 system at room temperature (300 K), to validate the force field through comparison with the experimental data from literature. The system has been equilibrated with the Berendsen barostat for 100 ns, a production step of 100 ns with the Parrinello-Rahman barostat was then performed. The cell parameters (see Tab. 1) were in good agreement with the experimental ones [6], while the simulated density (1109 g/L with a standard deviation of 6.635 g/L) slightly underestimates the experimental value (1133 g/L). The oreder parameter was also calculated and remained higher than 0.996 for the entire simulation, proving the stability of the molecular crystal.

	a	b	c
Exp. (293K)	5.927	7.880	29.18
Sim. Mean (300K)	6.130	8.036	28.26
Sim. Std (300K)	0.055	0.074	0.074
	α	β	γ
Exp. (293K)	90.00	92.44	90.00
Sim. Mean (300K)	90.02	90.97	89.99
Sim. Std (300K)	1.332	0.810	0.532

Table 1: Experimental values, averages and standard deviations of the crystalline cell parameters of the C_8-BTBT-C_8 crystal. The simulated values of a and b are the box parameters divided by 5, while the c parameter and the angles correspond to the experimental properties.

3.3. BTBT_50: Thermal behaviour and phase transitions

The following simulations were performed to study the thermal behaviour of the C_8-BTBT-C_8 crystal with increasing temperature and find eventual transitions, with the application of the Berendsen barostat. The BTBT_50 system has been simulated at 360 K for 100 ns, at 380 K for 200 ns, at 400 K 200 ns, at 420 K for 100 ns, at 450 K for 200 ns and at 500 K for 100 ns.
The simulation at 360 K did not present any transition from the crystalline phase. The simulation at 380 K yielded interesting results: the system is smectic until 75 ns, then forms separated lamellar domains up to 150 ns, then it is nematic. These observations from the trajectory are reinforced by the diagrams in Fig. 7 and 8. The formation of a smectic phase was expected, yet the lamellar domains and the nematic phase have not been experimentally observed [16, 17].

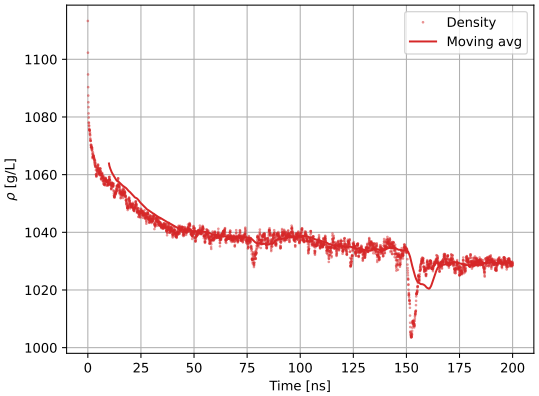

Figure 7: Diagram of the density for the BTBT_50 system at 380 K. The two transitions are evident as the density spikes to accommodate the change in structure.

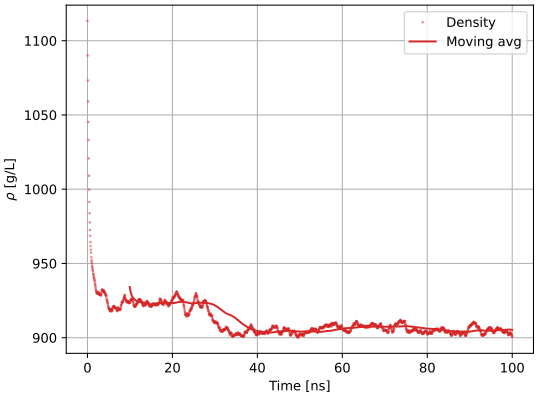

Figure 9: Time series of the density of BTBT_50 at 480 K. The drop at 28 ns indicates the transition to the liquid phase after a first stabilization.

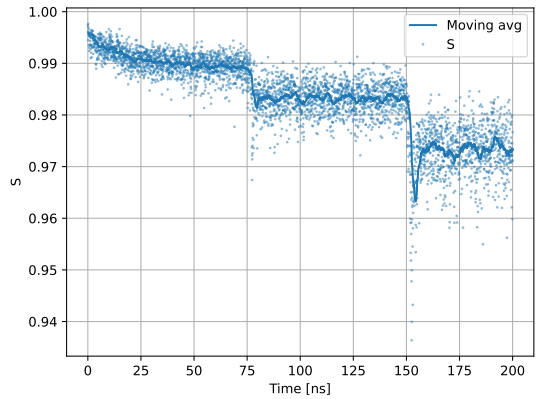

Figure 8: Diagram of the order parameter for the BTBT_50 system at 380 K. S decreases by steps through the transitions.

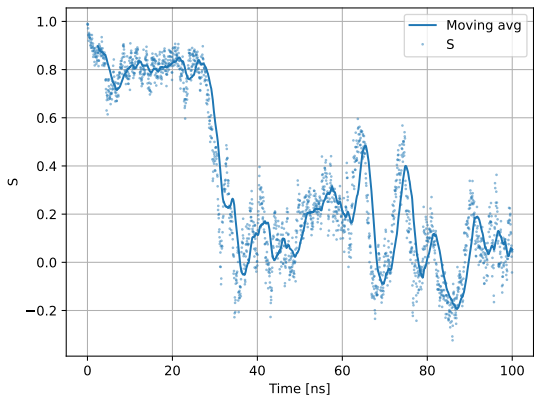

Figure 10: Time series of the order parameter of BTBT_50 at 480 K. After 28 ns S oscillates around 0.

In the simulation at 400 K, the BTBT_50 system shifts to a nematic phase at 20 ns, while the systems at 420 K and 450 K turn to nematic immediately. Finally, after 28 ns in the simulation of the system at 480 K, the melt point appears and the system becomes isotropic, as shown by the density and order parameter diagrams in Fig. 9 and 10. At 500 K, the system turns to isotropicity slightly sooner. Again, this behaviour is different from the literature: the melt point for C_8-BTBT-C_8 stands at around 396 K.

3.4. Q47: Simulation of C_8-BTBT-C_8 crystal on an a-SiO_2 surface

The final step of the study is the investigation of the layered structure of C_8-BTBT-C_8 on the surface of amorphous silica, by measure of the order parameter and height of the layers. In Tab. 2 a list of the performed simulations is shown.

Simulated Q47 systems

System	Temperature	Total time
Q47_200	300 K	40 ns
Q47_450	300 K	39.5 ns
Q47_450	400 K	40 ns
Q47_900	300 K	40 ns
Q47_900	500 K	33 ns

Table 2: Summary of simulated Q47 systems. Temperature and overall simulation time are reported.

The first simulations were performed at room temperature on the three systems. The Q47_200 system quickly loses its order, with peripheral molecules collapsing on the surface. While the order parameter remains higher than 0.95, the height reaches a value lower than 2 Å. The Q47_450 system, being larger, is more stable and remains higher. The measured measured height is 2.4 Å, which is comparable to the values found in the literature [7]. The Q47_900, double layer, system demonstrate that the two layers behave differently (Fig. 11 and 12): the first layer is still similar to the Q47_450 system, while the second layer is almost similar to the BTBT_50 system. The values of the height for both layers (respectively 2.5 Å and 2.8 Å), as well as the total height (5.3 Å) compare well with the experimental data [7, 18].

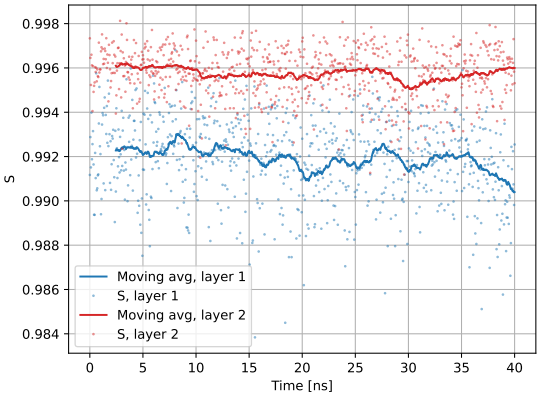

Figure 11: Order parameter in the Q47_900 system at 300 K, each plot represents a layer.

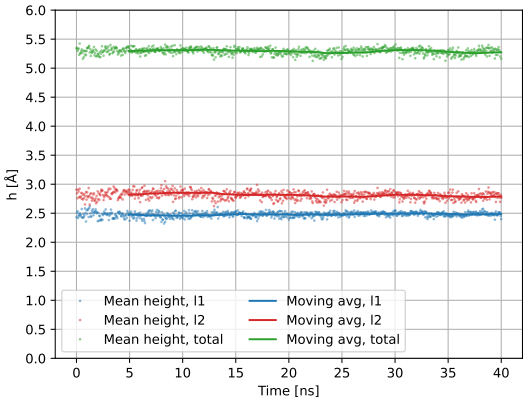

Figure 12: Mean height in the Q47_900 system at 300 K, each plot represents a layer. The plot for the second layer (red) specifically reports the effective total height of the two layers, not the height of the second one alone.

High temperature simulations were performed on the Q47_450 and the Q47_900 systems. The effect of temperature on the monolayer is the flattening of the molecules on the surface. At this temperature, the molecules are expected to start evaporating from the layer [16], yet this behaviour is not seen. Nonetheless, the system at 40 ns is still not at equilibrium. Even at 500 K, the BTBT molecules do not desorb from the surface. Instead, the molecules collapse on each other and form a continuous film on the surface.

4. Conclusions

The investigation of the thermal behaviour and the layered structure of C_8-BTBT-C_8 on amorphous silica, by use of MD, was the aim of this work. The force field was developed from the CHARMM 2021 FF [9, 19], adding the necessary terms for the interactions of C_8-BTBT-C_8 and the surface, with the aid of the CGenFF utility [20]. The generated FF proved to be suitable for this study after the simulation of BTBT_50 at 300 K, despite the weaker intermolecular interactions. Higher temperature simulations allowed to delineate the phase transitions. An unexpected configuration in the form of lamellar domains appeared at 380 K. Moreover, the melting point appeared only at 480 K. To better understand this behaviour, the simulation may have to be extended and simulations on larger systems may have to be executed. The room temperature simulations on the Q47 sys-

tems allowed to determine that larger systems tend to be more stable, since higher molecular order is found far from the boundaries. In fact, the larger systems are more comparable with experimental results. Higher temperature simulations showed that the FF may in fact exaggerate the interactions between the silica and the BTBT molecules, which do not evaporate, yet more knowledge on the surface chemistry in experimental studies is needed to make conclusions.
From this work, a series of improvements and new research paths arise. Better tools to analyse the results could provide new insights. Machine learning algorithms could be implemented to study the coordinates of the trajectories and find patterns. The simulations could be further extended, or new simulations could be performed at closer temperature intervals. Simulations on larger systems could also be done to identify size effects on the results.

5. Acknowledgements

I would like to express my gratitude towards my thesis supervisor, Prof. Mosè Casalegno.
Moreover, I am grateful to the CINECA consortium for the awarded computational resources, obtained through an ISCRA-C project grant.
This work is dedicated to my grandparents, which endured hardships for their families and allowed me to follow my dreams. A heartfelt thanks to my family, my friends and most of all, my girlfriend, for the continuous and unconditional support.

References

[1] Christopher Grieco, Grayson S. Doucette, Jason M. Munro, Eric R. Kennehan, Youngmin Lee, Adam Rimshaw, Marcia M. Payne, Nichole Wonderling, John E. Anthony, Ismaila Dabo, Enrique D. Gomez, and John B. Asbury. Triplet transfer mediates triplet pair separation during singlet fission in 6,13-Bis(triisopropylsilylethynyl)-Pentacene. *Advanced Functional Materials*, 27:1703929, 12 2017.

[2] Liwei Huang, Qing Liao, Qiang Shi, Hongbing Fu, Jinshi Ma, and Jiannian Yao. Rubrene micro-crystals from solution routes: their crystallography, morphology and optical properties. *J. Mater. Chem.*, 20:159–166, 2010.

[3] Marta Mas-Torrent, Peter Hadley, Stefan T. Bromley, Xavi Ribas, Judit Tarrés, Montserrat Mas, Elies Molins, Jaume Veciana, and Concepció Rovira. Correlation between crystal structure and mobility in organic field-effect transistors based on single crystals of tetrathiafulvalene derivatives. *Journal of the American Chemical Society*, 126:8546–8553, 7 2004.

[4] Shengzhong Liu, Ying-Jie Lu, Manfred M. Kappes, and James A. Ibers. The structure of the C60 molecule: X-Ray crystal structure determination of a twin at 110 K. *Science*, 254:408–410, 10 1991.

[5] E. Hädicke and F. Graser. Structures of eleven perylene-3,4:9,10-bis(dicarboximide) pigments. *Acta Crystallographica Section C Crystal Structure Communications*, 42:189–195, 2 1986.

[6] Takafumi Izawa, Eigo Miyazaki, and Kazuo Takimiya. Molecular ordering of high-performance soluble molecular semiconductors and re-evaluation of their field-effect transistor characteristics. *Advanced Materials*, 20:3388–3392, 7 2008.

[7] Michael Dohr, Oliver Werzer, Quan Shen, Ingo Salzmann, Christian Teichert, Christian Ruzié, Guillaume Schweicher, Yves Henri Geerts, Michele Sferrazza, and Roland Resel. Dynamics of monolayer-island transitions in 2,7-Dioctyl-benzothienobenzthiophene thin films. *ChemPhysChem*, 14:2554–2559, 8 2013.

[8] GROMACS website. `https://www.GROMACS.org`. Accessed: 2022-03-10.

[9] Fateme S. Emami, Valeria Puddu, Rajiv J. Berry, Vikas Varshney, Siddharth V. Patwardhan, Carole C. Perry, and Hendrik Heinz. Force field and a surface model database for silica to simulate interfacial properties in atomic resolution. *Chemistry of Materials*, 26:2647–2658, 4 2014.

[10] GALILEO100 page on the CINECA HPC website. `https://www.hpc.cineca.it/`

hardware/galileo100. Accessed: 2022-03-24.

[11] Charles R Harris, K Jarrod Millman, Stéfan J van der Walt, Ralf Gommers, Pauli Virtanen, David Cournapeau, Eric Wieser, Julian Taylor, Sebastian Berg, Nathaniel J Smith, Robert Kern, Matti Picus, Stephan Hoyer, Marten H van Kerkwijk, Matthew Brett, Allan Haldane, Jaime Fernández del Río, Mark Wiebe, Pearu Peterson, Pierre Gérard-Marchant, Kevin Sheppard, Tyler Reddy, Warren Weckesser, Hameer Abbasi, Christoph Gohlke, and Travis E Oliphant. Array programming with NumPy. *Nature*, 585:357, 2020.

[12] Jeff Reback, jbrockmendel, Wes McKinney, Joris Van den Bossche, Tom Augspurger, Phillip Cloud, Simon Hawkins, Matthew Roeschke, gfyoung, Sinhrks, Adam Klein, Patrick Hoefler, Terji Petersen, Jeff Tratner, Chang She, William Ayd, Shahar Naveh, JHM Darbyshire, Marc Garcia, Richard Shadrach, Jeremy Schendel, Andy Hayden, Daniel Saxton, Marco Edward Gorelli, Fangchen Li, Matthew Zeitlin, Vytautas Jancauskas, Ali McMaster, Pietro Battiston, and Skipper Seabold. pandas-dev/pandas: Pandas, February 2020.

[13] Wes McKinney. Data Structures for Statistical Computing in Python. In Stéfan van der Walt and Jarrod Millman, editors, *Proceedings of the 9th Python in Science Conference*, pages 56 – 61, 2010.

[14] J. D. Hunter. Matplotlib: A 2D graphics environment. *Computing in Science & Engineering*, 9(3):90–95, 2007.

[15] William Humphrey, Andrew Dalke, and Klaus Schulten. VMD – Visual Molecular Dynamics. *Journal of Molecular Graphics*, 14:33–38, 1996.

[16] M. Dohr, H. M. A. Ehmann, A. O. F. Jones, I. Salzmann, Q. Shen, C. Teichert, C. Ruzié, G. Schweicher, Y. H. Geerts, R. Resel, M. Sferrazza, and O. Werzer. Reversibility of temperature driven discrete layer-by-layer formation of dioctyl-benzothieno-benzothiophene films. *Soft Matter*, 13:2322–2329, 2017.

[17] Christos Grigoriadis, Claude Niebel, Christian Ruzié, Yves H. Geerts, and George Floudas. Order, viscoelastic, and dielectric properties of symmetric and asymmetric Alkyl[1]benzothieno[3,2-*b*][1]benzothiophenes. *The Journal of Physical Chemistry B*, 118:1443–1451, 2 2014.

[18] Lu Lyu, Dongmei Niu, Haipeng Xie, Yuan Zhao, Ningtong Cao, Hong Zhang, Yuhe Zhang, Peng Liu, and Yongli Gao. The correlations of the electronic structure and film growth of 2,7-diocty[1]benzothieno[3,2-*b*]benzothiophene (C8-BTBT) on SiO_2. *Physical Chemistry Chemical Physics*, 19:1669–1676, 2017.

[19] Academic CHARMM website. https://www.academiccharmm.org. Accessed: 2022-03-10.

[20] CGENFF website. https://cgenff.umaryland.edu/. Accessed: 2022-03-23.